

# Structural Systems Comparison of Simply Supported PSC Box Girder Bridge Equipped with Elastomeric Rubber Bearing and Lead Rubber Bearing

Santoso, A.<sup>1</sup>, Sulisty, D.<sup>1</sup>, Awaludin, A.<sup>1\*</sup>, Setiawan, A.F.<sup>1</sup>, Satyarno, I.<sup>1</sup>, Purnomo, P.<sup>2</sup>, and Harry, I.<sup>2</sup>

---

**Abstract:** This study compares the influence of elastomeric rubber bearing (ERB) as the regular bearing support and lead rubber bearing (LRB) as the seismic isolation device on the structural system of a seven simply supported span prestressed concrete (PSC) box girder bridge, which was analyzed using nonlinear time history analysis (NLTHA) with the OpenSees software. The results showed that the maximum pier responses and damage were smaller in models with LRB than with ERB. The bridge model using ERB showed the damage at level II, while the one using LRB was at level I. In addition, the highest seismic performance level in the model with ERB was at the operational limit state. Meanwhile, the seismic performance in the model with LRB was at the fully operational limit state. Thus, LRB performed better in improving the seismic performance and mitigating the damage due to the seismic excitation with the small cross-section area of pier.

**Keywords:** Box girder bridge; Pier; LRB; ERB; Seismic Performance; NLTHA.

---

## Introduction

Pier failure due to earthquake excitation causes a significant impact on the entire structure. It might cause the superstructure to collapse, increasing the cost of repairing or replacing the broken component. Struve Slough Bridge and Mission Gothic Bridge in California were two examples that collapsed due to Loma Prieta and Northridge Earthquake, respectively. Those were initiated by the pier collapse owing to the brittle shear failure [1]. Many bridges in Indonesia were designed using elastomeric rubber bearing (ERB), where the seismic capacity was lower than the bridge with a seismic isolation device. Therefore, the pier of the bridge with ERB would require large cross-section area to have an equitable seismic resistance with the other piers using seismic isolation device.

The seismic isolation device is widely employed to reduce the seismic responses by interposing the structural element with a low horizontal stiffness between the superstructure and substructure to decouple the structure from the horizontal component of ground motion [2].

It contributes to accommodating the earthquake force and dissipating the amount of seismic energy to control the seismic response of the structure [3]. The earthquake force can be reduced if the structural flexibility and structural damping are increased (e.g., the application of seismic isolator can lengthen the period) [4]. The common seismic isolators applied to the structure are lead rubber bearing (LRB) that provides lateral flexibility and damping capacity which is represented by an elastic-perfectly plastic bilinear response. The maximum deformation of LRB is 250% [4,5], while ERB is only 50% [6]. It implies that the LRB can deform more than ERB when subjects to the earthquake force.

Chen and Li [7] concluded that LRBs were capable of reducing the displacement between superstructure and substructure effectively. A numerical study by Edalathi and Tahghighi [8] showed that the application of LRB instead of ERB increased the structural flexibility, significantly reduced the base shear, bending moment, deck acceleration, pier displacement, and earthquake input energy of a continuous box girder bridge. Another study also showed that LRB significantly reduced the base shear of the suspension bridge [9] and the pier displacement of the continuous box girder bridge [10].

The seismic performance investigation of a simply supported bridge equipped with LRB compared to ERB has not been studied yet, despite the bridge's behavior being quite different from the continuous

---

<sup>1</sup> Department of Civil and Environmental Engineering, Gadjah Mada University, Yogyakarta, INDONESIA

<sup>2</sup> PT. Wijaya Karya Beton Tbk., Boyolali, INDONESIA

\*Corresponding author; Email: ali.awaludin@ugm.ac.id

**Note:** Discussion is expected before July, 1<sup>st</sup> 2022, and will be published in the "Civil Engineering Dimension", volume 24, number 2, September 2022.

Received 05 April 2022; revised 09 April 2022; accepted 11 April 2022.

bridge. The decks are not connected continuously, causing an increase in structural flexibility so that the dynamic responses might be more significant [11]. Hence, the study related to that topic is critical.

In this study, the comparison of structural system of simply supported prestressed concrete (PSC) box girder bridge equipped with LRB and ERB is investigated using numerical analysis. The bridge is located in Makassar, Indonesia, in seismic zone 3 or moderate-damage risk zone, and it is classified as a critical bridge according to the Indonesian code provision [12]. Nonlinear time history analysis (NLTHA) is carried out to simulate the dynamic responses of the structure by imposing five ground motions that are selected and scaled roughly similar to the designed spectral of the located bridge.

### Bridge Modeling

Figure 1 depicts a simply supported seven span PSC box girder bridge with a total length of 345 m, supported by a series of single pier with different heights. Two isolated bridge models equipped with ERB and LRB are considered in this analysis. To limit the deformation, Model A employs three ERBs in each deck support, shear key, and stopper as shown in Figure 2(a), whereas Model B employs only two LRBs in each deck support as shown in Figure 2(b). The existing bridge's structural system (Model B) is redesigned using a conventional system of ERB (Model A) with an equitable seismic resistant to the existing pier. Due to the low seismic capacity of ERB, the earthquake force will be much larger in Model A, necessitating a bigger pier dimension and more reinforcement than in Model B, as depicted in Figure 3.

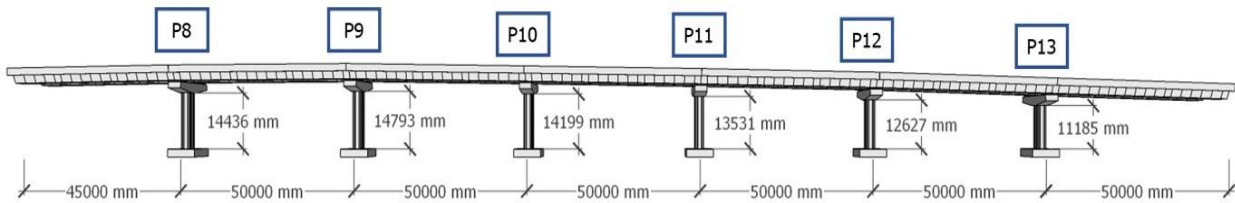


Figure 1. Longitudinal Section of the Bridge Model

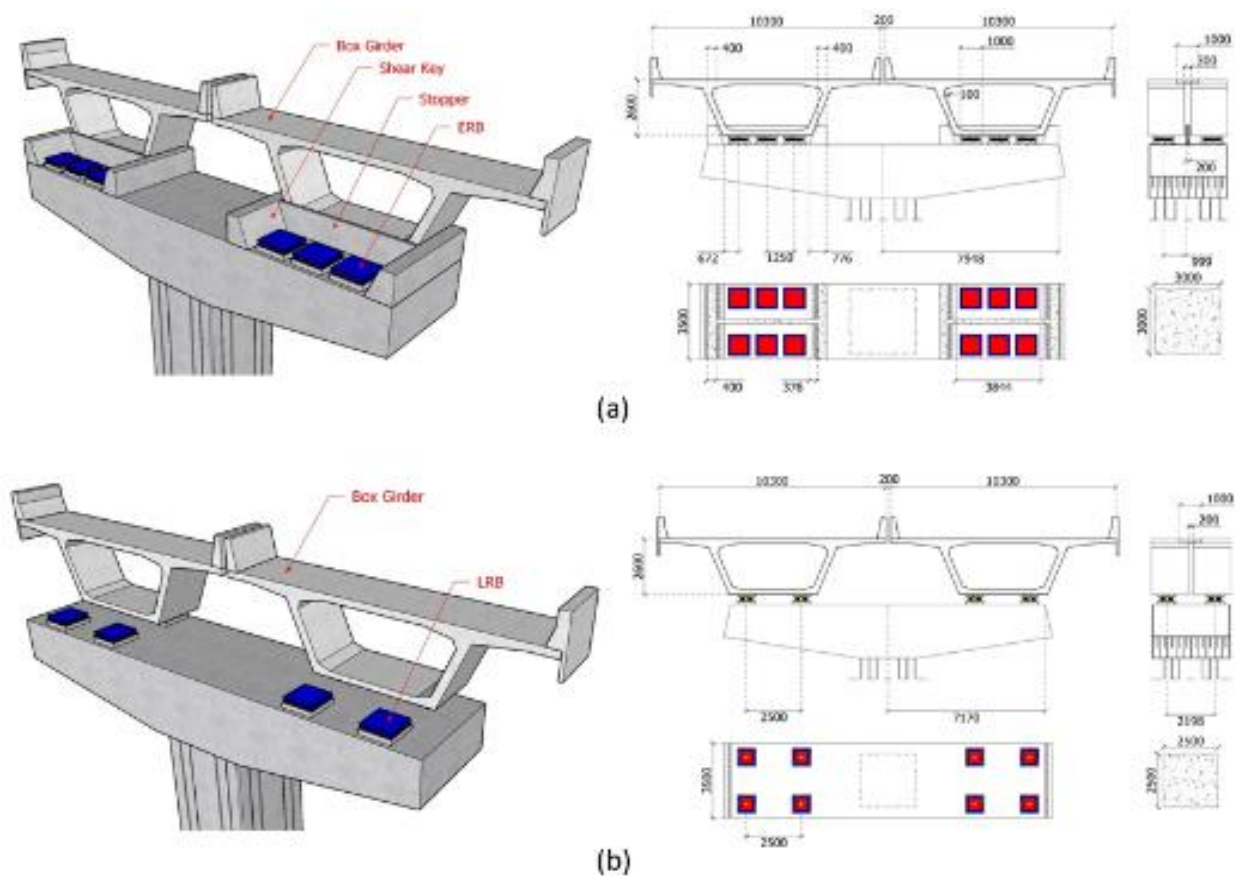


Figure 2. An Overview of the Bridge Model: (a) Model A; (b) Model B (unit in mm)

The bridge is modeled using Open Sees software. All elements except the pier are modeled as an elastic section, while the pier is modeled using a fiber section along the plastic hinge length ( $L_p$ ). It can be calculated as shown in Ref [13,14] using Equation (1), where  $L$  is the column length,  $f_{ye}$  is the expected yield strength of longitudinal reinforcing steel bar, and  $d_{bl}$  is the nominal diameter of longitudinal reinforcing steel bar.

$$L_p = 0.08L + 0.022f_{ye}d_{bl} \geq 0.044f_{ye}d_{bl} \text{ (mm, MPa)} \quad (1)$$

Both elastic and fiber sections are modeled as force-based beam-column elements (FBE) with the distributed-plasticity model, assuming the plasticity is spread along the entire element length to accurately calculate the bending moment by integrating the force-deformation response [15]. The element discretization is required to localize the deformation and represent the curvature distribution along with the element [16]. Therefore, five integration points of the Gauss-Lobatto integration rule are applied at the elastic element. For the integration point for the pier the Hinge-Radau integration rule is used, which is concentrated along the plastic hinge length [17]. The applied axial load may affect large deformation to the structure, so the geometric nonlinearity effect is also considered in this analysis.

Nonlinear material parameters for concrete and reinforcing steel are considered in this analysis. The concrete materials are calculated according to Mander's model [18] for confined and unconfined

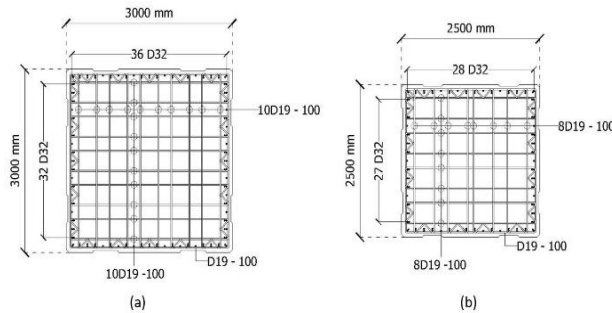


**Figure 3.** The Reinforcement Details: (a) Model A; (b) Model B

**Table 1.** *Concrete04* Material Properties

Model	Concrete	$f_c$ (MPa)	$\epsilon_c$	$\epsilon_{cu}$	$E_c$ (MPa)	$f_{ct}$ (MPa)	$\epsilon_t$
A and B	Unconfined	33.20	0.0020	0.0050	28,809.7	3.59	0.0011
A	Confined	57.86	0.0094	0.0305	38,032.3	3.59	0.0011
B	Confined	57.82	0.0094	0.0308	38,020.6	3.59	0.0011

**Table 2.** *Steel02* and *MinMax* Material Properties

Model	$f_y$ (MPa)	$R_0$	$CR1$	$CR2$	$b$	$E_0$ (MPa)	$\epsilon_{min}$	$\epsilon_{max}$
A and B	490	20	0.925	0.15	0.01	200,000	-0.11	0.11

concrete in compression, while Vecchio-Collins' model [19] is considered for tensile concrete. It is defined as *Concrete04*, where the parameters are listed in Table 1, such as the concrete maximum stress ( $f_c$ ), concrete strain at maximum stress ( $\epsilon_c$ ), concrete strain at crushing strength ( $\epsilon_{cu}$ ), the elastic modulus of concrete ( $E_c$ ), the maximum tensile strength ( $f_t$ ), and the ultimate tensile strain of concrete ( $\epsilon_t$ ).

The steel parameters are idealized as *Steel02* according to Giuffre-Menegotto-Pinto's model [20,21] that also consider the ultimate strain using *MinMax* material. The input parameters in the OpenSees are yield strength ( $f_y$ ), initial curvature between initial and post-yield curve ( $R_0$ ), curvature variation parameter of Bauschinger effect ( $CR1$  and  $CR2$ ), the ratio between post-yield and elastic stiffness ( $b$ ), the elastic modulus of steel ( $E_0$ ), and ultimate strain at the bilinear response ( $\epsilon_{min}$  and  $\epsilon_{max}$ ).

Two node-link elements idealize ERB, LRB, shear key, stopper, link slab, gap, and foundation. Meanwhile, a zero-length element with elastic material is used to perform a rigid connection between the link element and the other element or link. It assumes very high stiffness (*i.e.*,  $10^{14}$  N/mm) in the six degrees of freedom. The shear key, stopper, link slab, and gap of 200 mm are modeled using elastic-perfectly plastic material with gap (*ElasticPPGap*) in the OpenSees considering the pounding effect assuming that they will perform an elastic behavior on the pounding occurrence [22]. The nine-pile of the foundation is idealized to be a linear spring element and is assumed to be a rigid foundation and flexible soil [23-25].

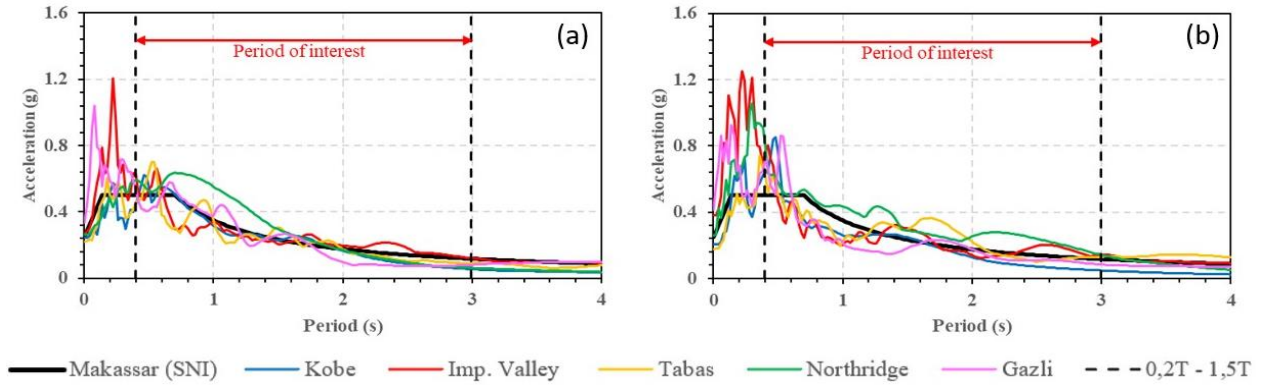
According to AASHTO LRFD (2012), the preliminary design is carried out to calculate the ERB's parameter, while the LRB's parameters are calculated based on AASHTO GSID (2014) and a detailed engineering drawing of the existing bridge. Those are idealized as force-displacement curves with the input parameters are summarized in Table 3. Where  $F_y$  is the yield force,  $K_u$  is the initial stiffness,  $K_d/K_u$  is the ratio between post-yield and initial stiffness,  $d_y$  is the yield displacement,  $d_{isol}$  is the maximum displacement capacity,  $K_v$  is the vertical stiffness,  $K_{rx}$ ,  $K_{ry}$ , and  $K_{rz}$  are rotational stiffness in x, y, and z-axis.

**Table 3.** ERB and LRB Material Properties

Component	$F_y$ (kN)	$K_u$ (kN/mm)	$K_d / K_u$	$d_y$ (mm)	$d_{sol}$ (mm)	$K_v$ (kN/mm)	$K_{rx}$ (kN/mm)	$K_{ry}$ (kN/mm)	$K_{rz}$ (kN/mm)
ERB	259.20	14.40	0.05	-	18	11,964.44	$2.55 \times 10^9$	$2.55 \times 10^9$	$3.07 \times 10^6$
LRB	275.10	15.97	0.16	17.23	195	6444.67	$6.50 \times 10^8$	$6.50 \times 10^8$	$3.17 \times 10^5$

**Table 4.** Five Records of Ground Motions Selected

No	Earthquake	Station	Fault	$M_w$	$V_{s30}$ (m/s)	R (km)	Scale Factor (SF)	
							SF <sub>x</sub>	SF <sub>y</sub>
1	Kobe	Takarazuka	Strike-slip	6.90	312.00	38.60	0.35	0.34
2	Imperial Valley	El Centro Array #13	Strike-slip	6.53	249.92	21.98	2.29	2.75
3	Tabas	Boshrooyeh	Reverse	7.35	324.57	74.66	2.09	2.10
4	Northridge	Rinaldi Receiving Sta	Reverse	6.69	282.25	10.91	0.30	0.50
5	Gazli	Karakyr	Reverse	6.80	259.59	12.81	0.48	0.48

**Figure 4.** The Scaled Elastic Response Spectral in: (a) Longitudinal; (b) Transverse Directions

### Ground Motion Modification

Five records of ground motions selected in this analysis (Table 4) are classified as a far-fault earthquake with epicentral distances greater than 10 km. The ground motion selection considers the spectral shape that is roughly similar to the Makassar earthquake, so the other provisions such as magnitude ( $M_w$ ), fault distance ( $R$ ), source mechanism, fault type, and site condition can be relaxed [26]. Nevertheless, the magnitude  $\geq 5$ , fault distance  $\leq 500$  km, shallow crustal mechanism, strike-slip, and reverse fault, and site class D are still be considered based on the BMKG earthquake repository [27] that were explained in the study by Sunardi and Nugraha [28] due to a lack of references regarding deaggregation of Makassar Earthquake. The amplitude scaling method is carried out to modify the ground motion selected. This method applies a single scale factor to the entire ground motion record to preserve the variation of earthquake energy with the fundamental period found in the original record [26]. The scale factor ( $SF$ ) is calculated using the proposal of Kalkan and Chopra [29] at Equation (2).

$$SF = \left( \sum_{i=1}^n \bar{A}_i A_i \right) / \left( \sum_{i=1}^n A_i A_i \right) \quad (2)$$

Where  $\bar{A}_i$  and  $A_i$  are the target and record (unscaled) spectral acceleration at the  $i^{th}$  spectral period at the period of interest, respectively. The period of interest for scaling must be scaled between  $0.2T_1$  and  $1.5T_1$ , where  $T_1$  represents the fundamental period at the first mode, and  $n$  is the number of periods at the period range. The scaled elastic response spectral for each pair of ground motion are depicted in Figure 4.

### Limit States

The seismic performance investigation aims to assess the damaged component by classifying performance and damage level based on the limit state from the previous report [1]. The limit state is divided into five damage levels, where the slightest damage is classified as damage level I, which is equivalent to fully operational. Otherwise, the largest damage is classified as damage level V, equivalent to collapse [1]. In addition, the damage level from I to IV indicates that the bridge or certain components are still repairable. Meanwhile, the damage level V indicates that the bridge or some components require significant repair or even component replacement. The complete description about limit states can be found in Table 5.

**Table 5.** Limit States According to NCHRP Synthesis 440 [1]

Damage Level	Damage Descriptions	Performance Level	Steel Strain	Concrete Strain	% Drift
I	The onset of hairlines cracks	Fully operational	0.0038	0.0024	0.75%
II	Crack widening, first yield of longitudinal reinforcement	Operational	0.005	0.0032	1%
III	Inelastic deformation, cover concrete spalling, diagonal crack occurs	Life safety	0.019	0.01	3%
IV	Tha crack and the concrete spalling become wider	Near collapse	0.048	0.027	5%
V	Buckling of longitudinal reinforcement, rupture of transverse reinforcement, and crushing of core concrete	Collapse	0.063	0.036	8.7%

## Results and Discussion

### The Difference in Structural Systems

The preliminary design of the pier was carried out in the model with ERB using a single-mode spectral approach according to the code provision [23]. The designed earthquake force was larger in Model A (with ERB) than in Model B (with LRB). The spectral acceleration was reduced in the model with LRB by increasing the structural flexibility represented by the fundamental period. As a result, the fundamental periods of Model A were 2.01 s in the transverse and 1.09 s in the longitudinal direction of the translation mode. Meanwhile, there were 2.50 s and 1.91 s of Model B's periods in transverse and longitudinal directions, respectively. The fundamental period of Model A was less than Model B, indicating that the structure was stiffer in Model A. Consequently, the lateral force and bending moment on the pier became larger so that increase the pier's size and the number of reinforcements. Eventually, the pier in Model A became stronger than in Model B. As a result, the shear and bending moment capacities of the pier in Model A were 38,736.69 kN and 105,909.8 kNm, while they were 31,545.0 kN and 68,509.23 kNm in Model B, respectively.

### Dynamic Responses

The stiffness provided by a series of the piers in the longitudinal causes smaller responses in the longitudinal than in the transverse. Furthermore, Model A is also supported by the stopper (longitudinal) and shear key (transverse), which provide lateral support to confine the deck from moving and transmit the lateral shear force to save the pier. The reduction percentage is obtained from the relative of the maximum response from models with ERB and LRB to the maximum response of ERB. Thus, it can describe the effectivity of the the seismic isolation device (LRB) to reduce the seismic responses compared to the conventional bearing (ERB).

Based on Figure 5, the displacement due to longitudinal earthquakes exhibits similar results in Model A, while Model B shows varied results.

The highest and the shortest pier are represented by pier P9 and P13, respectively, from the six piers in this study. The higher the pier, the less stiffness is provided. Therefore, in the series of piers with different heights, the highest pier will be the most flexible to move rather than the shortest one. A significant reduction is clearly shown in P13, while the least reduction is shown in P9. As presented in Table 6, the highest percentage of displacement reduction is 51.79% at the shortest pier due to the Tabas Earthquake. Unfortunately, the LRB cannot reduce the displacement due to the Gazli Earthquake even though the pier responses are much smaller than the other ones.

Rather than in the longitudinal (X) direction, a single cantilever pier consideration provides less stiffness in the transverse (Y) direction. The highest percentage of displacement reduction due to the transverse earthquake is shown at pier P10. It equates to 43.14% as presented in Table 6. Otherwise, the maximum displacement of piers on edge (P8 and P13) is relatively small, while the LRB cannot reduce some earthquakes at piers on edge. It signifies that the transverse earthquakes influence the middle pier more than the edge, and the LRB reduces the displacement effectively in the larger responses rather than, the smaller ones.

The percentage of base shear reduction can be found in Table 7. Based on the results, LRB can significantly reduce the base shear in longitudinal (X) and transverse (Y) directions, as depicted in Figure 6. The highest percentage reaches 80.38% in the longitudinal and 67.66% in the transverse direction. Both results are located at pier P12 due to the Tabas Earthquake. In contrast, the lowest percentage of 40.37% is shown at pier P10 due to the Gazli Earthquake in the longitudinal, and 18.37% at pier P8 due to the Imperial Valley Earthquake in the transverse. As depicted in Figure 6, the base shear in both directions is still below the maximum capacity of 38,736.69 kN and 31,544.99 kN for the models with ERB and LRB, respectively. It means that all piers will not fail due to shear failure.

**Table 6.** Displacement Reduction in Longitudinal (X) and Transverse (Y) Direction

Pier	Displacement Reduction (%)									
	Kobe		Imperial Valley		Tabas		Northridge		Gazli	
	X	Y	X	Y	X	Y	X	Y	X	Y
P8	11.98	14.80	3.30	-	32.76	12.01	0.17	-	-	8.70
P9	-	12.77	0.06	-	27.40	15.76	3.70	16.42	-	30.85
P10	6.83	17.63	2.04	10.74	33.24	31.90	10.01	36.04	-	43.14
P11	13.96	22.81	4.70	-	38.75	18.40	7.58	13.92	-	21.78
P12	17.45	23.22	10.07	14.87	41.11	28.65	9.73	33.80	-	13.70
P13	33.31	35.76	25.08	-	51.79	-	23.89	16.69	-	7.95

Note: The symbol “-“ means that the seismic response is not reduced.

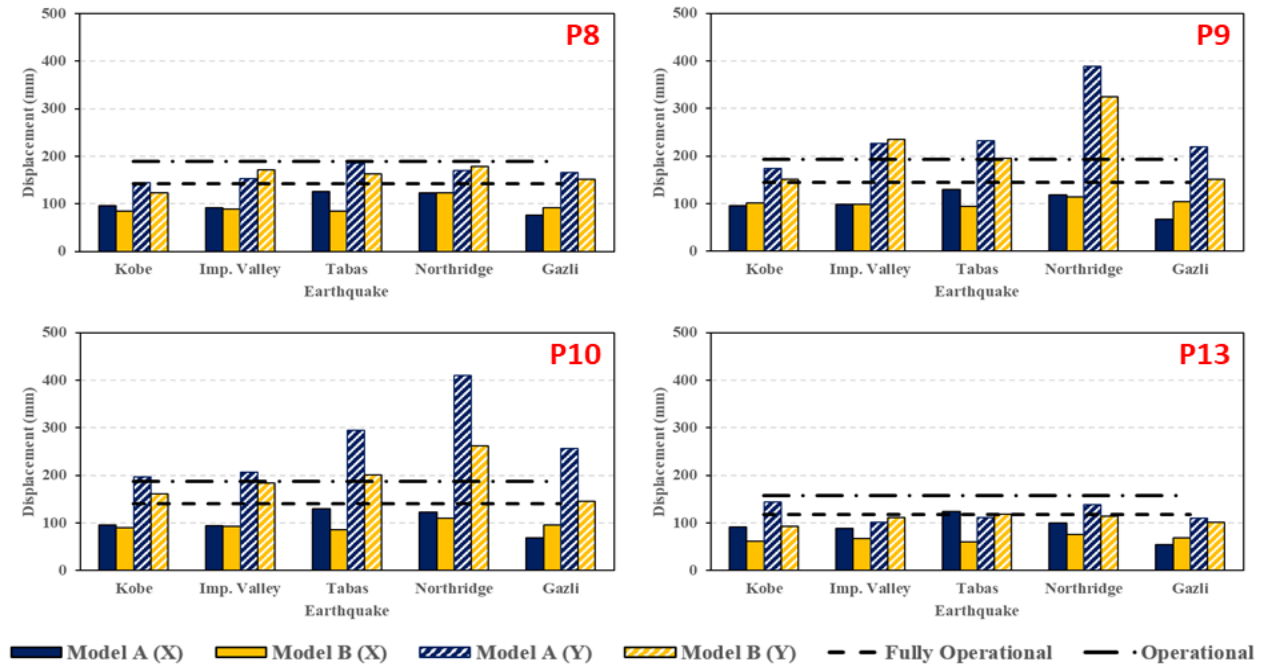


**Figure 5.** Pier Maximum Displacement Comparison in Models A and B

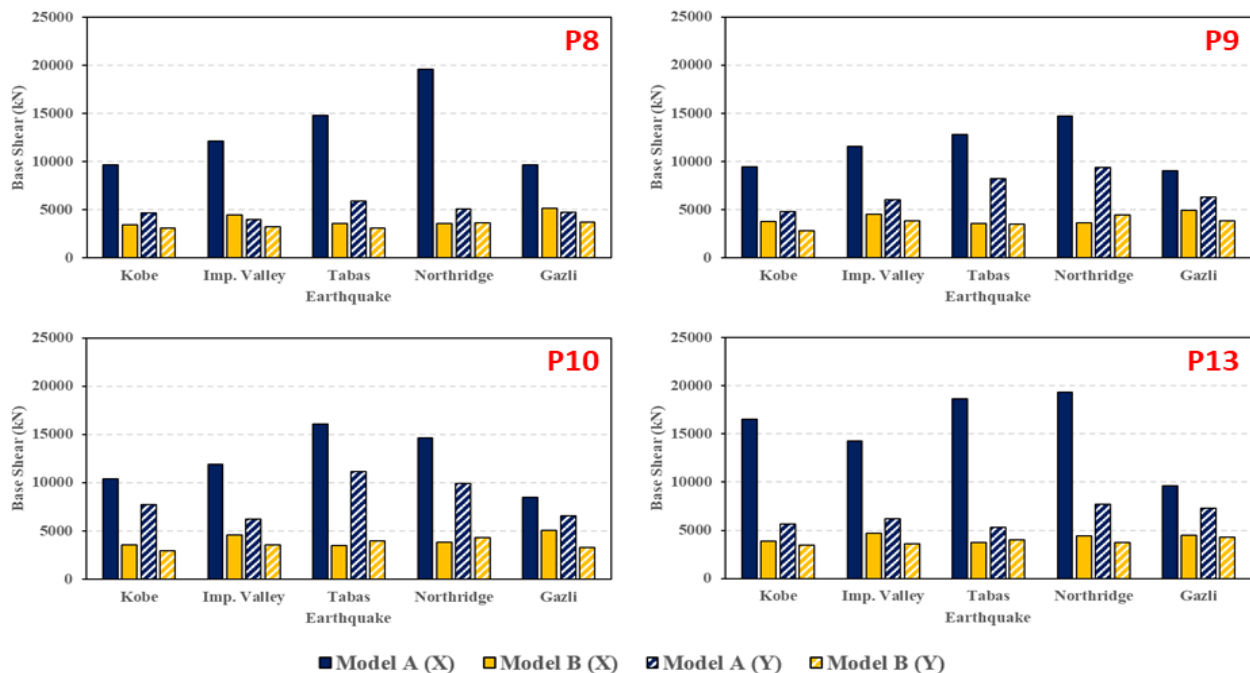


**Figure 6.** Maximum Base Shear Comparison of Models A and B

**Table 7.** Base Shear Reduction in Longitudinal (X) and Transverse (Y) Direction

Pier	Base Shear Reduction (%)									
	Kobe		Imperial Valley		Tabas		Northridge		Gazli	
	X	Y	X	Y	X	Y	X	Y	X	Y
P8	64.24	34.40	62.97	18.40	75.73	47.20	81.36	28.44	46.89	22.79
P9	59.90	42.15	60.96	36.82	72.13	57.41	75.44	52.73	45.75	38.59
P10	65.61	62.03	61.34	43.53	78.40	64.53	74.10	56.77	40.37	50.61
P11	71.36	35.74	59.64	21.50	73.74	60.52	73.33	51.71	43.76	35.68
P12	76.41	60.66	67.84	33.45	80.38	67.66	65.50	42.19	42.85	38.54
P13	76.41	38.04	67.01	41.59	79.99	24.10	77.25	51.26	53.22	41.44

Note: the symbol “-“ means that the seismic response is not reduced.

**Table 8.** Bending Moment Reduction in Longitudinal (X) and Transverse (Y) Direction

Pier	Bending Moment Reduction (%)									
	Kobe		Imperial Valley		Tabas		Northridge		Gazli	
	X	Y	X	Y	X	Y	X	Y	X	Y
P8	24.68	32.00	21.28	13.51	14.85	30.42	27.49	17.69	7.13	27.88
P9	14.54	30.59	22.81	23.19	5.57	33.47	22.88	33.46	-	43.41
P10	23.17	35.90	23.53	23.89	-	58.10	27.20	36.97	-	51.49
P11	29.04	36.18	21.70	4.32	-	33.22	27.17	32.61	-	36.67
P12	30.12	36.42	24.78	31.00	-	36.46	23.95	40.11	-	29.85
P13	40.78	43.43	32.24	11.82	2.06	14.51	36.96	31.61	-	22.98

Note: the symbol “-“ means that the seismic response is not reduced.

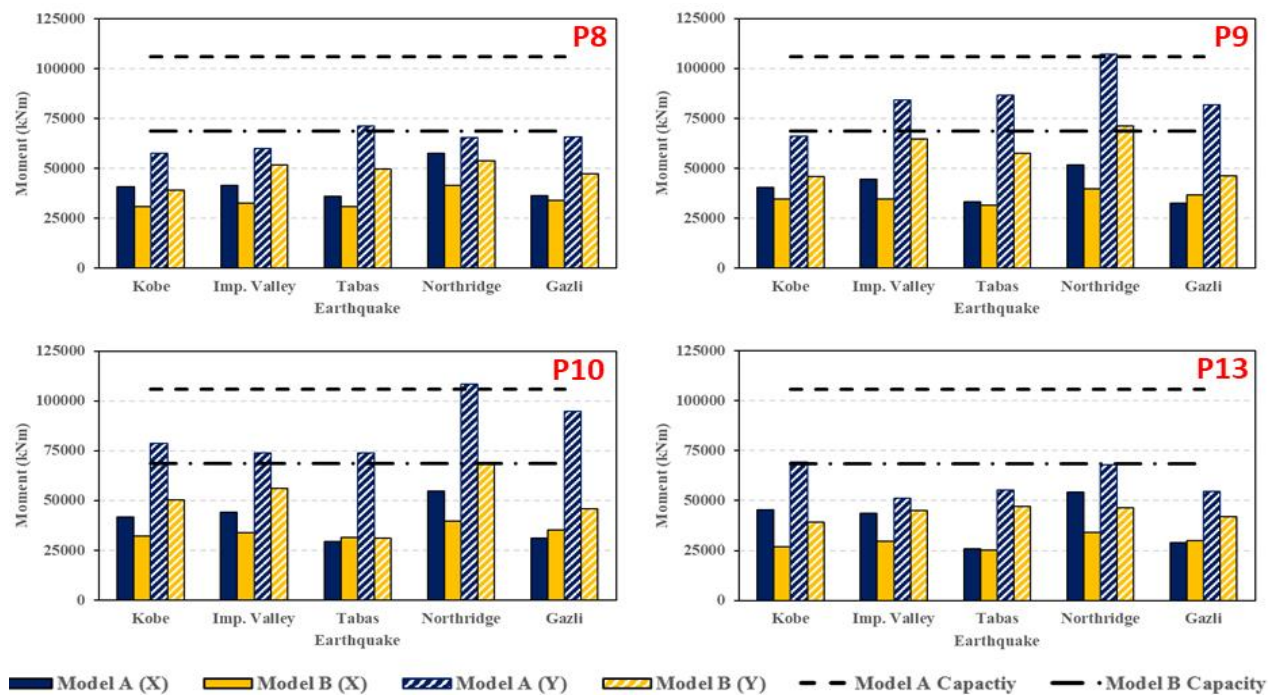


**Figure 7.** Maximum Bending Moment Comparison of Model A and B

LRB performed better to reduce the bending moment due to transverse earthquakes rather than longitudinal ones. Five-moment responses in the transverse direction can be reduced consistently, with the highest percentage of 58.10% shown at pier P10 due to the Tabas Earthquake. At the same time, 40.78% of bending moment reduction is shown at pier P13 due to the Kobe Earthquake in the longitudinal direction. Unfortunately, some earthquakes, such as Tabas and Gazli, failed to be reduced. However, they exhibit smaller bending moments than the others, as presented in Figure 7.

All bending moments due to longitudinal earthquakes are not exceed the maximum capacities in Models A and B. Still, the bending moments that occurred at piers P9 and P10 due to the Northridge Earthquake slightly exceeded the bending moment capacity of the pier in Model A. Regarding the moment responses at Model B, pier P9 is the only one that slightly exceeds the maximum capacity of the pier for the model with seismic devices. Thus, LRB also performs well to avoid flexural failure. Table 8 shows the bending moment reduction through the use of LRB.

### Pier Damage

The damage levels are determined by equating displacement and curvature to the drift percentage corresponding to the provision in Table 5. The curvatures are observed along the plastic hinge length from the bottom of the pier. All results are represented by some pier in the edge (*i.e.*, pier P8 and P13) and in the middle (*i.e.*, pier P9 and P10) to exhibit the severity of pier damage. The results of the four piers are depicted in Figure 8.

The pier damage due to the longitudinal earthquake in Models A and B is still below damage level I, except for pier P8 in Model A, which includes damage level II. It implies that LRB can minimize the damage due to longitudinal earthquakes by keeping the damage to a hairline crack occurrence. Otherwise, the results of transverse earthquakes are larger and vary, whereby the largest damage in Models A and B occurs on piers P10 and P9, respectively. The damages in both piers are classified as damage level III, where it initiates the onset of cover concrete spalling, inelastic

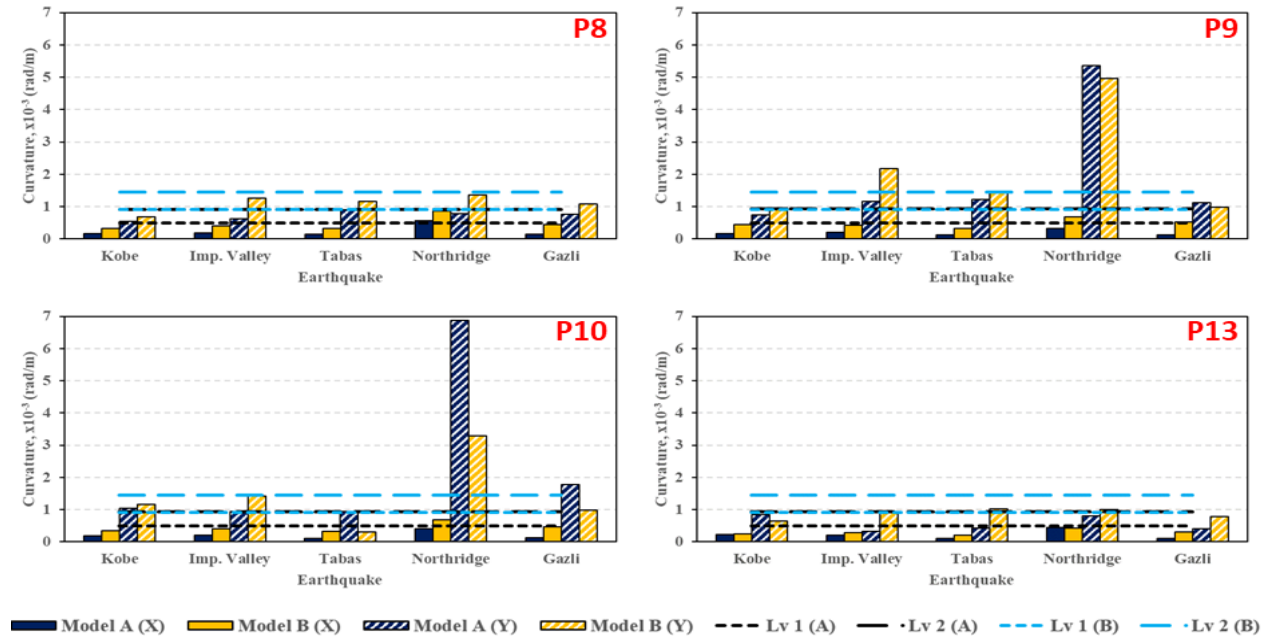


Figure 8. Maximum Curvature Comparison of Models A and B

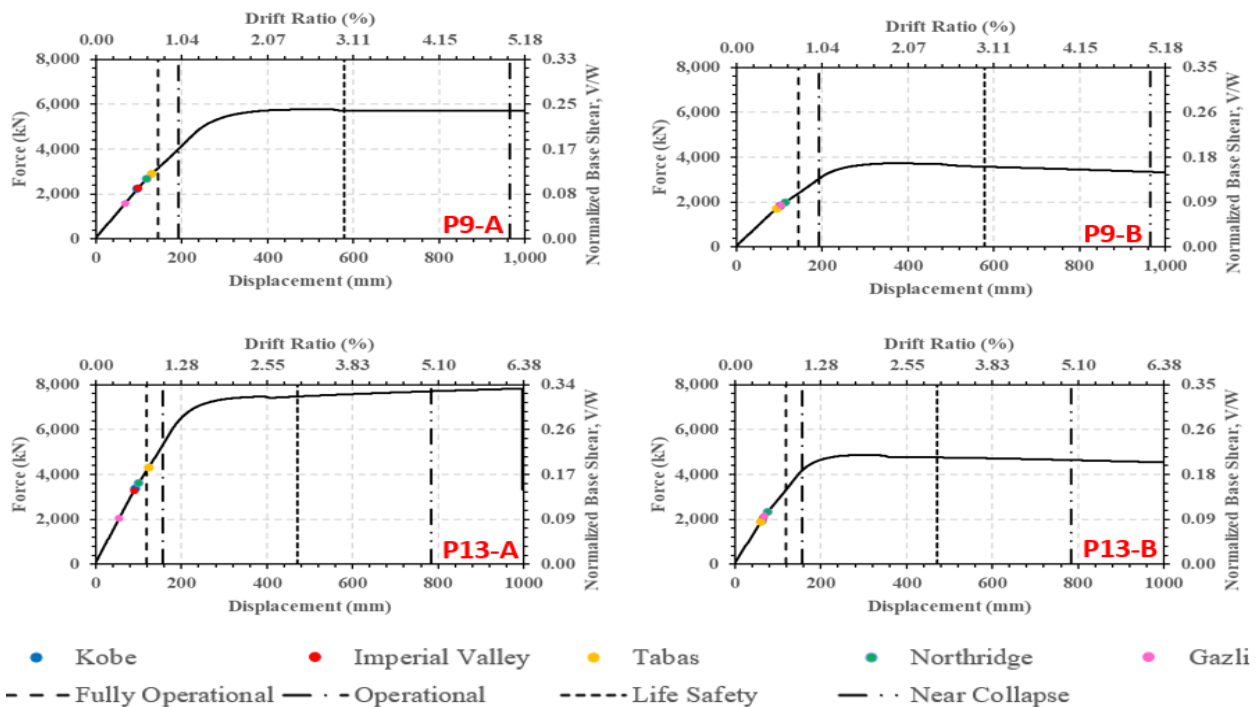


Figure 9. Pier Performance in Models A and B due to Longitudinal Earthquakes

deformation, and the development of diagonal cracks. The transverse earthquake, particularly the Northridge, clearly caused more damage to piers in the middle rather than at the edge. Even though the

damage in the model with LRB cannot be reduced significantly in the small responses, the damages that appeared in the large responses are less than in the model with ERB.

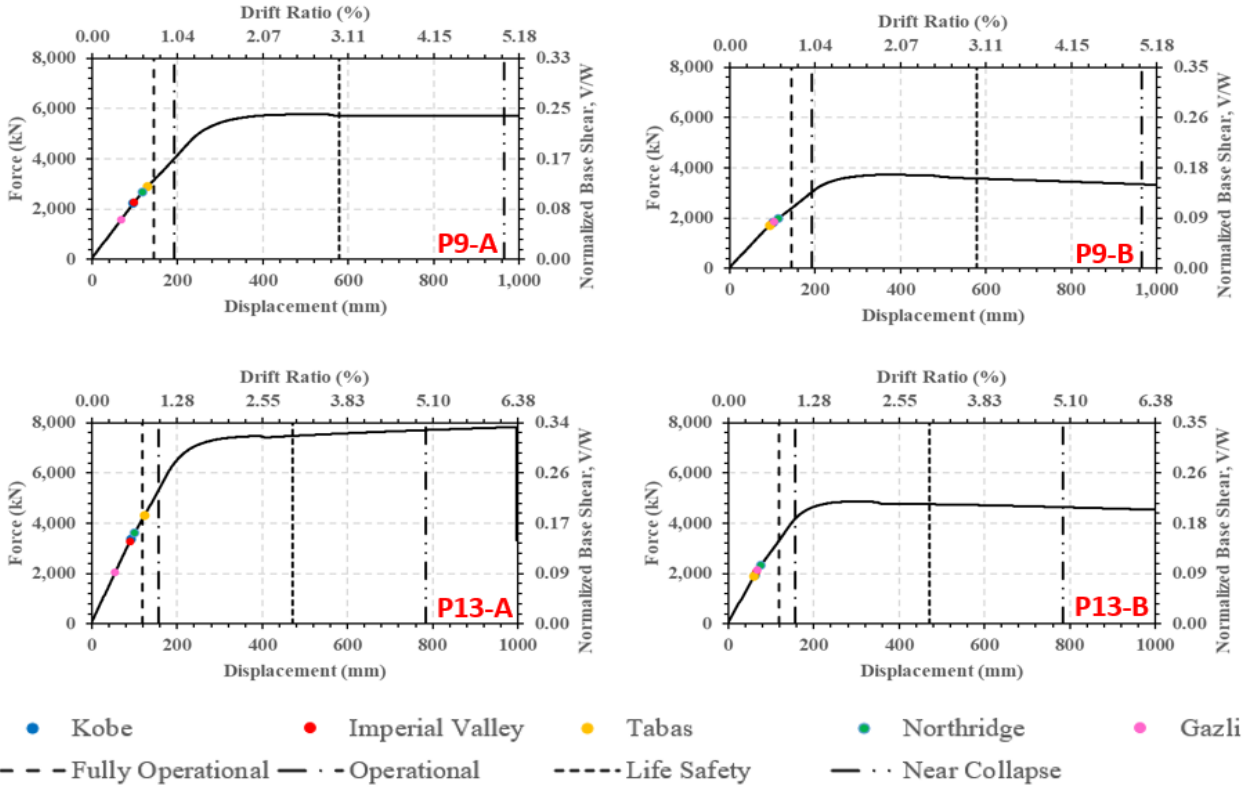


Figure 9. Pier Performance in Models A and B due to Longitudinal Earthquakes

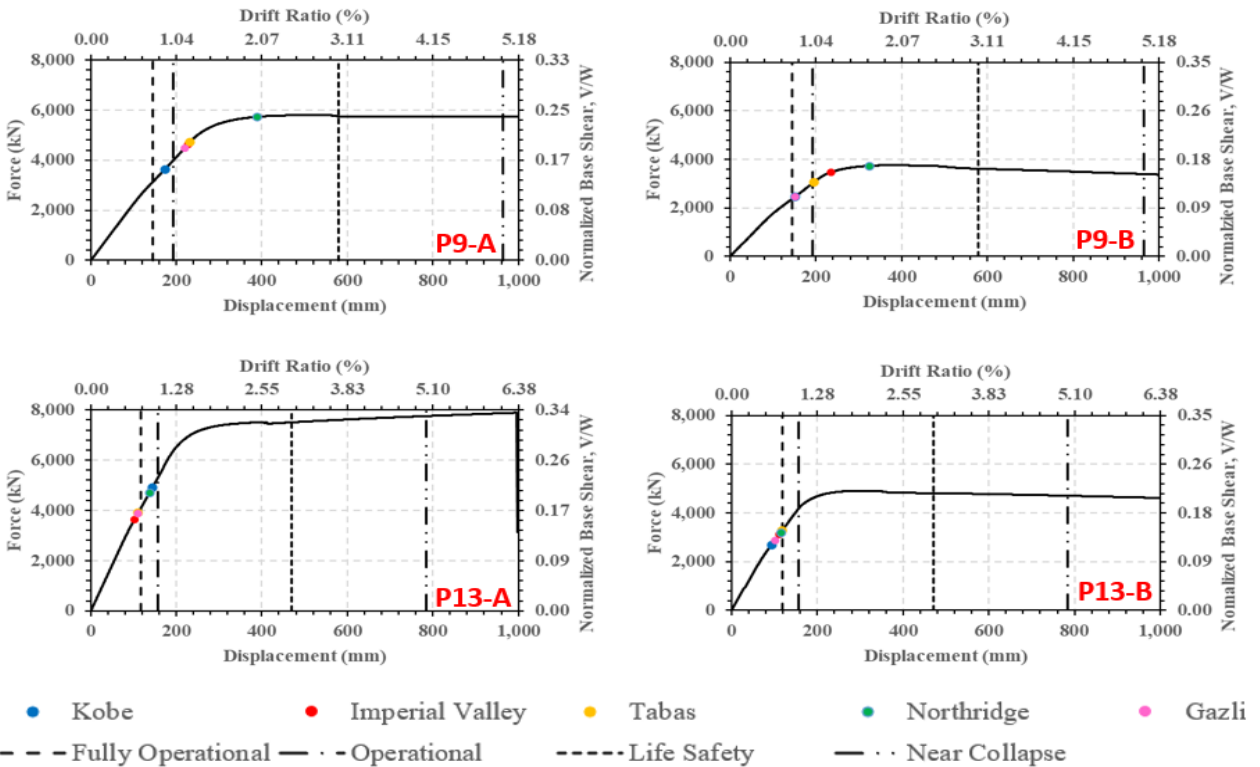


Figure 10. Pier Performance in Models A and B due to Transverse Earthquakes

### Pier Performances

The pier performance represents the bridge’s capability to operate after the designed earthquake occurrence, classified into five performance levels as presented in Table 5. The performance level is represented by the position of the performance point in the capacity curve obtained from the maximum

displacement of each pier due to the designed earthquakes. The capacity curve is obtained from the pushover analysis to perform the static nonlinear response of each pier.

Figure 9 depicts the pier performance of Model A and B due to longitudinal earthquakes. The results show that the bridge with LRB exhibits good performance

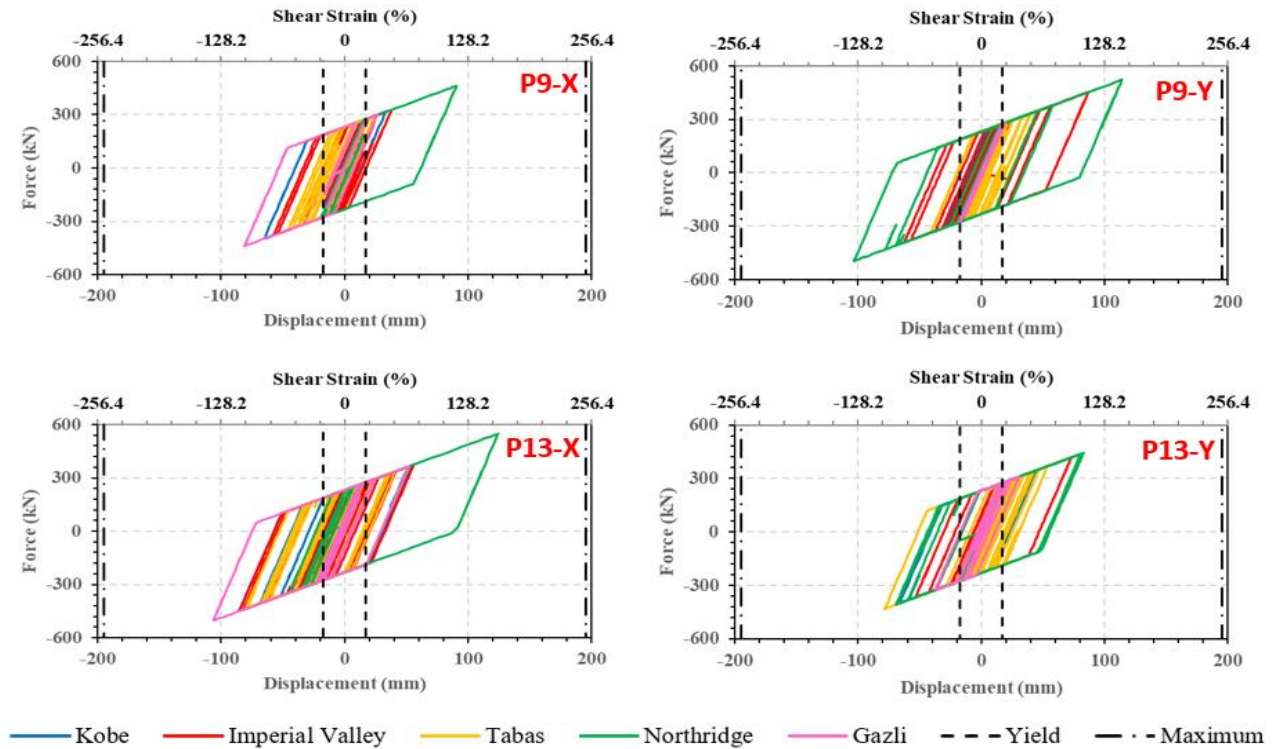


Figure 11. LRB Responses due to Longitudinal and Transverse Earthquakes

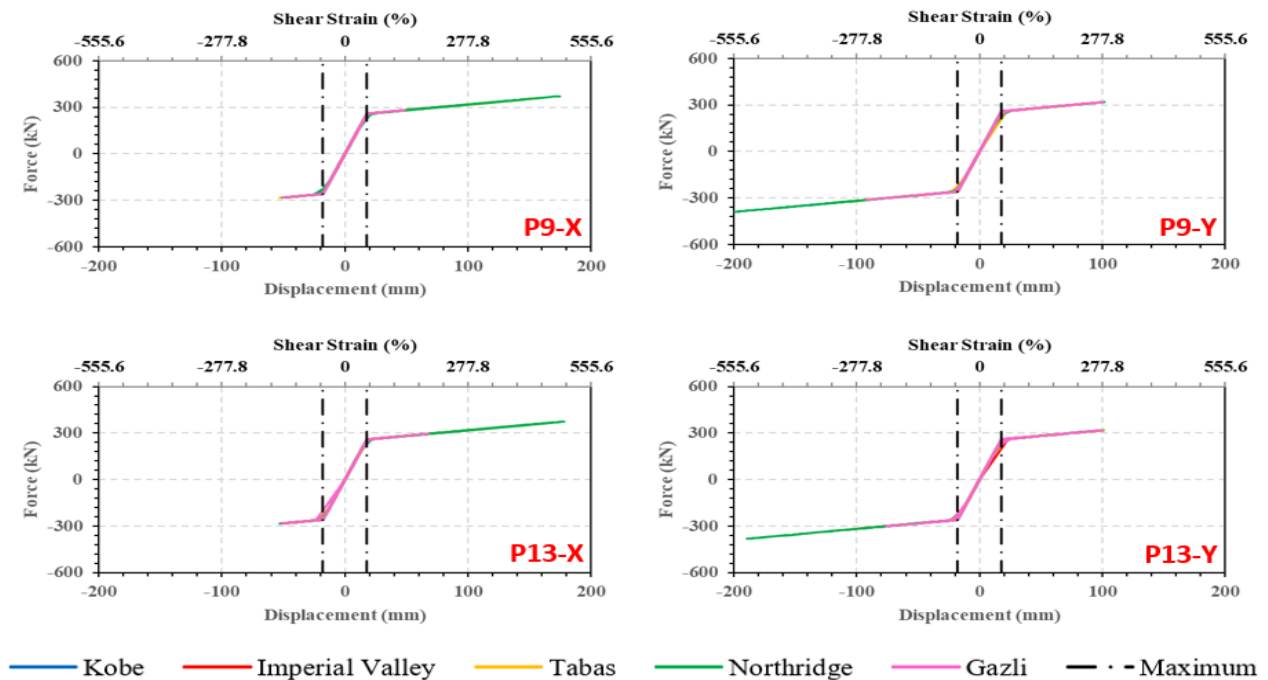


Figure 12. ERB Responses due to Longitudinal and Transverse Earthquakes

in both piers in the middle (P9) and the edge (P13). Those are still on the fully operational limit in the longitudinal direction. In the transverse (Figure 10), most performance points formerly located at the life safety limit change into the operational limit due to the application of LRB. Some performance levels roughly remain unchanged, but LRB reduces the lateral displacement due to certain earthquakes.

### Bearing Responses

The hysteresis curve represents the behavior of each bearing due to the designed earthquakes, which is shown as a force-displacement curve. While the LRB performs an elastic-perfectly plastic bilinear response, the ERB performs an elastic bilinear response. Figure 11 depicts the responses of the LRB on several piers due to the longitudinal and transverse earthquakes, respectively. As a result, the shear strains of LRB do not exceed the maximum shear strain of 250%, which is determined by the code [4]. The post-yield stiffness of LRB provides an adequate lateral restraint to perform an inelastic deformation after the initial stiffness has been exceeded. Thus, it implies that all LRBs can still be used, despite being affected by the earthquakes. Otherwise, the ERB's maximum shear strain is only 50%, while all ERBs have exceeded it. In addition, the lateral restraint of the ERB relies on the initial stiffness provided by the rubber. After it exceeds the initial stiffness, the post-yield stiffness is assumed to have only 5% of the initial stiffness, and the rubber is also torn. Thus, it implies that all ERBs need a replacement due to the designed earthquake occurrence. The results of ERB due to longitudinal and transverse earthquakes can be found in Figure 12, respectively.

### Conclusion

The bridge with ERB showed a shorter natural period than with LRB, indicating that the bridge was stiffer while utilizing ERB on the structural system. As a result, the dynamic responses of the pier (e.g., displacement, base shear, and moment) were greater than those of the pier in the bridge with LRB, necessitating a larger cross-section area and additional reinforcements to provide an equitable seismic resistant structure. Therefore, the damage and performance levels did not clearly show the difference between the two models. The damage level in both models due to the transverse earthquakes was shown to be the same at damage level III. However, damage level II was shown in the bridge equipped with ERB, while the other ones with LRB showed damage level I due to the longitudinal earthquakes. Similarly, in the pier performance levels, the results were exhibited at the operational limit state in the model with ERB and the fully operational limit in the model with

LRB in the longitudinal direction, but the life safety limit states were shown in both models in the transverse.

LRB performed better to reduce the seismic responses than the ERB. As a result, the pier displacement, base shear, and bending moment were reduced by using LRB up to 51.79%, 80.38%, and 58.10%, respectively. However, none of the LRBs exceeded the maximum shear strain of 250%. Otherwise, all ERBs exceeded the 50% shear strain limit. It indicated that the LRB was better at accommodating the horizontal load without any component replacement.

### Acknowledgments

The authors would like to gratefully acknowledge the Department of Civil and Environmental Engineering Gadjah Mada University and PT. Wijaya Karya Beton Tbk. for the data support for this study.

### References

1. NCHRP, *Performance-Based Seismic Bridge Design*, National Cooperative Highway Research Program, 2013.
2. Naeim, F. and Kelly, J.M., *Design of Seismic Isolated Structures: From Theory to Practice*, John Wiley & Sons Ltd., Chichester, 1999.
3. Hameed, A., Koo, M.S., Do, T.D., and Jeong, J.H., Effects of Lead Rubber Bearing Characteristic on The Response on Seismic-Isolated Bridge, *Journal of Civil Engineering*, 12, 2008, pp. 187-196, retrived from <https://doi.org/10.1007/s12205-008-0187-9>.
4. AASHTO, *Guide for Seismic Isolation Design*, American Association of State Highway and Transportation Officials, 2014
5. EN, *Anti-seismic Devices*, European Committee for Standardization, 2009.
6. AASHTO, *AASHTO LRFD Bridge Design Specification, Customary U.S. Units*, American Association of State Highway and Transportation Officials, 2012.
7. Chen, X. and Li, C., Seismic Performance of Tall Pier Bridges Retrofitted with Lead Rubber Bearings and Rocking Foundation, *Engineering Structures*, 212, 2020, pp. 1-15, retrived from <https://doi.org/10.1016/j.engstruct.2020.110529>.
8. Edalathi, A.A. and Tahghighi, H., Investigating the Performance of Isolation Systems in Improving the Seismic Behavior of Urban Bridges, A Case Study on The Hesarak Bridge, *Archives of Civil Engineering*, 65, 2019, pp. 155-175, retrived from <https://doi.org/10.2478/ace-2019-0052>.
9. Sugihardjo, H., Tavio, Manalu, I., and Lesmana, Y., Seismic Study of Lead-Rubber Bearing Application in Kutai Kartanegara Steel Arch

- Bridge, *Advance Science Engineering Information Technology*, 8, 2018, pp. 540-546, retrived from <https://doi.org/10.18517/ijaseit.8.2.4348>
10. Kim, W., Ahn, D. and Lee, J., A Study on the Seismic Isolation Systems of Bridges with Lead Rubber Bearings, *Open Journal of Civil Engineering*, 4, 2014, pp. 361-372, retrived from <https://doi.org/10.4236/ojce.2014.44031>.
  11. Nielson, B.G. and DesRoches, R., Seismic Performance Assessment of Simply Supported and Continuous Multispan Concrete Girder Highway Bridges, *Journal of Bridge Engineering*, 12, 2007, pp. 611-620.
  12. BSN, *Perencanaan Jembatan Terhadap Beban Gempa*, Badan Standardisasi Nasional, 2016.
  13. Paulay, T. and Priestley, M.J.N., *Seismic Design of Reinforced Concrete and Masonry Buildings*, John Wiley & Sons Ltd., 1992.
  14. AASHTO, *Guide Specifications for LRFD Seismic Bridge Design*. American Association of State Highway and Transportation Officials, 2011.
  15. Berry, M.P. and Eberhard, M.O., *Performance Modeling Strategies for Modern Reinforced Concrete Bridge Columns*, Pacific Earthquake Engineering Research Center, 2008.
  16. Scott, M.H. and Fenves, G.L., Plastic Hinge Integration Methods for Force-Based Beam-Column Elements, *Journal of Structural Engineering*, 132, 2006, pp. 244-252, retrived from [https://doi.org/10.1061/\(ASCE\)0733-9445\(2006\)132:2\(244\)](https://doi.org/10.1061/(ASCE)0733-9445(2006)132:2(244)).
  17. Kappos, A.J., Saiidi, M.S., Aydinoglu, M.N., and Isacovic, T., *Seismic Design and Assessment of Bridges*, Springer, 2012.
  18. Mander, J.B., Priestley, M.J.N., and Park, R., Theoretical Stress-Strain Model for Confined Concrete, *Journal of Structural Engineering*, 114, 1988, pp. 1804-1826, retrived from [https://doi.org/10.1061/\(ASCE\)0733-9445\(1988\)114:8\(1804\)](https://doi.org/10.1061/(ASCE)0733-9445(1988)114:8(1804)).
  19. Vechio, F.J. and Collins, M.P., The Modified Compression-Field Theory for Reinforced Concrete Elements Subject to Shear, *Journal of Structural Engineering*, 112, 1986, pp. 224-237, retrived from [https://doi.org/10.1061/\(ASCE\)0733-9445\(1986\)112:2\(224\)](https://doi.org/10.1061/(ASCE)0733-9445(1986)112:2(224)).
  20. Filippou, F.C., Popov, E.P., and Bertero, V.V., *Effect of Bond Deterioration on Hysteretic Behavior of Reinforced Concrete Joints*, Report EERC 83-19, Earthquake Engineering Research Center, University of California, 1983.
  21. Limbert, J., Afshan, S., Kashani, M.M., and Robinson, A.F., Compressive Stress-strain Behavior of Stainless Steel Reinforcing Bars with The Effect of Inelastic Buckling, *Engineering Structures*, 237, 2021, pp. 1-15.
  22. Omrani, R., et al., *Guidelines for Nonlinear Seismic Analysis of Ordinary Bridges: Version 2.0*. Caltran Final Report No. CA15-2266, California Departement of Transportation, University of California, 2015.
  23. ASCE, *Seismic Evaluation and Retrofit of Existing Buildings*, American Society of Civil Engineers, 2017.
  24. Bowles, J.E., *Foundation Analysis and Design, 5th Edition*, The McGraw-Hill Companies, Inc., 1974.
  25. Hardiyatmo, H.C., *Analisis dan Perancangan Fondasi II, 4th Edition*, Gadjah Mada University Press, 2018.
  26. ASCE, *Minimum Design Loads for Buildings and Other Structures*, American Society of Civil Engineers, 2010.
  27. BMKG, *Katalog Gempa Bumi*, 2022, retrived from [http://repogempa.bmkg.go.id/repo\\_new/](http://repogempa.bmkg.go.id/repo_new/).
  28. Sunardi, B. and Nugraha, J., Peak Ground Acceleration at Surface and Spectral Acceleration for Makassar City Based on A Probabilistic Approach, *Jurnal Meteorologi dan Geofisika*, 17, 2016, pp. 33-46.
  29. Kalkan, E. and Chopra, A.K., *Practical Guidelines to Select and Scale Earthquake Records for Nonlinear Response History Analysis of Structures*, U.S. Geological Survey Open-File Report 2010-1068, 2010, retrived from <https://doi.org/10.3133/ofr20101>.